ELSEVIER

Journal of Nuclear Materials 313–316 (2003) 11–22

journal of nuclear materials

www.elsevier.com/locate/jnucmat

Key ITER plasma edge and plasma–material interaction issues

G. Federici [a,*], P. Andrew [b], P. Barabaschi [a], J. Brooks [c], R. Doerner [d], A. Geier [e], A. Herrmann [e], G. Janeschitz [f], K. Krieger [e], A. Kukushkin [a], A. Loarte [g], R. Neu [e], G. Saibene [g], M. Shimada [h], G. Strohmayer [a], M. Sugihara [h]

[a] *ITER JWS Garching Co-center, Boltzmannstraße 2, 85748 Garching, Germany*
[b] *JET Joint Undertaking, Abingdon, Oxfordshire, OX14 3EA, UK*
[c] *Argonne National Laboratory, 9700 S. Cass Ave., Argonne, IL 60439, USA*
[d] *University of California San Diego, La Jolla, CA 92093-0417, USA*
[e] *Max-Planck-Institut fuer Plasmaphysik, 85748 Garching, Germany*
[f] *Forschungszentrum Karlsruhe, 76021 Karlsruhe, Germany*
[g] *EFDA Close Support Unit, Boltzmannstraße 2, 85748 Garching, Germany*
[h] *ITER Naka Joint Work Site, 801-1 Mukouyama, Naka-machi, Naka-gun 311-0193, Japan*

Abstract

Some of the remaining crucial plasma edge physics and plasma–material interaction issues of the ITER tokamak are discussed in this paper, using either modelling or projections of experimental results from existing tokamak operation or relevant laboratory simulations. The paper covers the following subject areas at issue in the design of the ITER device: (1) plasma thermal loads during Type I ELMs and disruptions, ensuing erosion effects and prospects for mitigating measures, (2) control of co-deposited tritium inventory when carbon is used even on small areas in the divertor near the strike points, (3) efficiency of edge and core fuelling for expected pedestal densities in ITER, and (4) erosion and impurity transport with a full tungsten divertor. Directions and priorities of future research are proposed to narrow remaining uncertainties in the above areas.

PACS: 52.40.H
Keywords: Plasma–wall interaction; Divertor; Boundary plasmas; ITER; Plasma-edge physics; B2-EIRENE code

1. Introduction

The capability to design a next-step DT burning plasma experiment has greatly expanded during the past two decades thanks mainly to remarkable improvements in plasma performance and control in today's machines and advances in various areas of physics and engineering. Integrating and extending these advances toward long pulsed or steady-state burning plasmas is now the focus of international tokamak research, which is ready to proceed to the construction of ITER as a physics and technology integration step.

Designing a robust interface between a thermonuclear plasma and the solid material environment remains, nonetheless, a major challenge for the success of ITER and for future fusion power reactors. Critical plasma boundary and plasma–material interaction (PMI) issues, where major gaps in our present understanding remain and extrapolations to ITER are uncertain include: (i) transient peak thermal loads during Type I edge localised modes (ELMs) and disruptions, (ii) control of co-deposited tritium inventory when carbon is used even on small areas in the divertor near the strike points, (iii) efficiency of edge and core fuelling for

* Corresponding author. Tel.: +49-89 3299 4228; fax: +49-89 3299 4110.
E-mail address: federig@ipp.mpg.de (G. Federici).

0022-3115/03/$ - see front matter © 2003 Published by Elsevier Science B.V.
PII: S0022-3115(02)01327-2

expected pedestal density (n_{ped}), and (iv) erosion and impurity transport of a full tungsten divertor.

This paper highlights what is presently known in these areas and assesses how accurately resulting effects and consequences for the design and operation of ITER can be predicted. Although this paper touches on most key aspects, there are a number of important areas, which for space limitation cannot be covered here, in particular the problems of dust and limiter erosion during plasma start-up. Moreover, since at this stage the conditions at the operating point for steady-state operation are somewhat unclear, most of the considerations in this paper refer to inductive operation in ITER. Section 2 briefly outlines the ITER design, expected performance, and the plasma-facing materials. Section 3 expands upon critical plasma edge and PMI issues and discusses results of modelling predictions for ITER and their implications on operation/performance. Section 4 suggests directions and priorities for further R&D. Finally, a summary is provided in Section 5.

2. ITER design

2.1. Objectives

ITER will be the first fusion device with significant Q (the ratio of fusion power to additional heating power) and extended burn [1]. The completion of the ITER Engineering Design Activities, in July 2001, has brought a mature design, cost estimate and safety analysis, that are supported by a body of validating physics and technology R&D [2]. A thorough discussion of the key physics performance issues can be found elsewhere [3–5]. The longer pulse duration and cumulative run-time, together with the higher heat loads during normal operation and more intense disruptions, represent the largest changes in operation conditions compared to today's experiments. Erosion of plasma-facing components (PFCs) over many pulses and distribution of eroded material, are critical issues that will affect the performance and the operating schedule of the ITER tokamak. Primary effects ensuing from erosion/re-deposition include plasma contamination, tritium co-deposition with carbon (if used in some parts of the divertor), component lifetime, dust, and formation of mixed-materials, whose behaviour is still uncertain. The relevant PMIs are comprehensively reviewed in [6].

2.2. Plasma-facing materials and divertor design optimisations

Currently, the ITER design employs several plasma-facing materials selected for their suitability to regions of the vessel with different power and particle flux characteristics. Beryllium is the primary candidate material for the first-wall, whereas tungsten is the preferred material for the divertor, except for the area near the strike-points where carbon will be used. Each of these three candidate materials has some inherent advantages and disadvantages [6], and their application depends on the specific operational requirements [7,8]. CFC is primarily chosen because of its high-thermal shock resistance and tolerance to off-normal events, since the operational lifetime of alternative materials such as tungsten in this region has significant uncertainties due to melt layer loss during disruptions and Type I ELMs.

Design choices in ITER have been made that are consistent with nuclear technology and remote maintenance requirements. In particular, the divertor is being designed to be very versatile, with components mounted onto removable and reusable cassettes. To enhance the compatibility with Type I ELMs thermal loads, a further inclination of the divertor target (e.g., using a factor of two smaller poloidal angle of magnetic field lines at the target surfaces), which would increase the plasma wetted area during ELMs, is being considered. The main drawback of this solution is that it negatively affects the operational flexibility of the machine by reducing the freedom of positioning the strike points.

In addition, the ITER divertor design is being further developed and optimised, based on new understanding of hydrocarbon formation, transport and deposition [9,10] with the scope to ameliorate the problem of controlling tritium in the carbon co-deposits. Several design options are currently being investigated to minimise the formation of films in specific areas e.g., by ensuring that regions of probable deposition are kept 'hot' during operation, leading to reduced tritium retention [11], or by enhancing deposition in specially designed 'cold traps' for the hydrocarbons ($\sim$70 K) [12], which could be periodically heated to recover the tritium in the form of stable gas molecules. Detailed evaluations of these designs are on-going.

To address the tritium-co-deposition concern, primarily associated with the use of carbon, ITER will maintain the option to switch from CFC to W armour on the divertor targets prior to DT operation. This change will depend on both the frequency and severity of ELMs and disruptions in the initial H/D plasmas, and the success of mitigating by design the occurrence of tritium co-deposition and/or on the availability of effective in situ tritium removal techniques.

3. Outstanding plasma edge and plasma–material interaction issues

3.1. Type I ELM energy losses in ITER and alternative scenarios

The reference regime for inductive operation in ITER is the ELMy H-mode with densities 80–90% of

the Greenwald density, which has been observed reliably and reproducibly in many tokamaks. One of the primary physics issues relating to plasma performance in the ELMy H-mode regime is the occurrence of Type I ELMs, which lead to large particle and power fluxes onto the divertor plates and expel from the core plasma (on average) ~30% of the input power [13,14]. Although heat loads to the divertor target during Type I ELMs are of no concern for present experiments, they may represent a major limitation for the divertor target lifetime of ITER and of future burning plasma experiments. Because, Type I ELMs are expected to occur with a frequency of the order of 1 Hz (i.e., few hundred ELMs per ITER pulse), if the power losses are such that the target surface temperature exceeds the sublimation (for carbon) or melting temperature (for tungsten), the predicted material erosion would lead to an unacceptable reduction of the divertor target lifetime (e.g., 3000 full performance pulses for the first ITER divertor).

3.1.1. Divertor thermal loads during Type I ELMs and ensuing erosion effects

A brief mention is made below to some important experimental observations on Type I ELMs, which impact the design of the ITER divertor and the erosion lifetime estimates. A comprehensive discussion on this subject can be found elsewhere [15].

- *ELM energy losses*: The analysis of the ELM energy loss data obtained across machines shows that the energy loss during Type I ELMs (ΔW_{ELM}) is proportional to the energy in the H-mode pedestal (W_{ped}) and is correlated with the pedestal plasma collisionality (ν^*_{ped}), with smaller ELM energy losses (<10% of the pedestal energy) occurring at higher collisionality, or with parallel transport time $\tau_{\|}$ [16], or, possibly, with pedestal density normalised to the Greenwald density (n_{ped}/n_{GW}) [15]. Present evidence points towards a better correlation of $\Delta W_{ELM}/W_{ped}$ with ν^*_{ped} than with n_{ped}/n_{GW}. On the basis of scaling with ν^*_{ped} (in ITER ~0.04) the expected $\Delta W_{ELM}/W_{ped}$ in ITER would be ~15–20%. On the basis of scaling with $\tau_{\|}$ (~240 μs in ITER) the expected $\Delta W_{ELM}/W_{ped}$ would be ~10–15%. Finally, if the parameter that determines $\Delta W_{ELM}/W_{ped}$ is n_{ped}/n_{GW}, the expected $\Delta W_{ELM}/W_{ped}$ would be ~4–5%.
- *Asymmetries in power deposition*: The few reported observations indicate that the ELM power deposition is, on average, toroidally symmetric with a typical 30% scattering around perfect toroidal symmetry [17]. The measured inboard/outboard observed divertor asymmetry vary from experiment to experiment, being typically 3 to 1 in ASDEX-Upgrade [17–19] and 1 to 1 in JET and DIII-D [17,20]. At present it is not clear if the experimentally observed asymmetry is due to the interpretation of the infra-red (IR) measurements, which particularly for JET, can be complicated for the inner divertor due to the existence of thick re-deposited carbon layers. Similarly, the percentage of the energy lost from the plasma that reaches the divertor is seen to be in the range of 50–100%. Whether this ratio depends on plasma conditions or is just due to the random component of the ELM energy deposition is not know at the moment. Large ELM fluxes onto the main chamber walls (more than 20 cm away form the separatrix) have been observed in tokamaks [21], with a phenomenology similar to the blobby transport in the SOL [22].
- *Wetted area*: It is larger than that of the power deposition in-between ELMs but the broadening is not very large (~1.5–2 in JET and ASDEX-Upgrade) [18,20]. At present, it is not known whether the broadening of the power deposition profile at the target during ELMs depends on pedestal plasma conditions or if the scatter in the data reflects the statistical nature of the ELM event.
- *ELM duration*: The analysis of the experimental data from tokamaks show that the time for energy deposition is possibly determined by the transport of energy form the pedestal to the divertor target along open field lines ($\tau_{\|} = 2\pi R q_{95}$). In particular, the rise time for the surface target temperature as measured by IR at the target (τ_{IR}) in JET, ASDEX-Upgrade and JT-60U, is very well-correlated with $\tau_{\|}$ with a typical ratio of $\tau_{IR}/\tau_{\|}$~1.5–3.0 for a $\tau_{\|}$~240 μs, as expected in ITER [13]. Analysis of the time dependence of the power load during a Type I ELM in JET and ASDEX-Upgrade [18,20] reveals that a non-negligible amount of the ELM energy (30–50%) reaches the target when the temperature of the divertor target has already started to decrease, and hence the duration of the power load is significantly longer than τ_{IR} by a factor ~1.5–3.0. Furthermore, this observation indicates that the approximation taken in the past of a square power load of duration τ_{IR} to calculate the divertor power loads and target temperature, overestimates considerably the expected temperature rise of the divertor target surface [23].

3.1.2. Estimates of target erosion lifetime during ELMs

The critical parameters that determine the acceptability of ELMs for the divertor target from the erosion standpoint are the pedestal energy content, the fraction of pedestal stored energy loss, the fraction of this energy that reaches the divertor plate (including asymmetries), the effective wetted area, including broadening of the power width, the duration and shape of the ELM power load pulse. The knowledge of these quantities and the extrapolation of the ELM behaviour to ITER are still uncertain at present in large part due to the difficulty of the associated measurements.

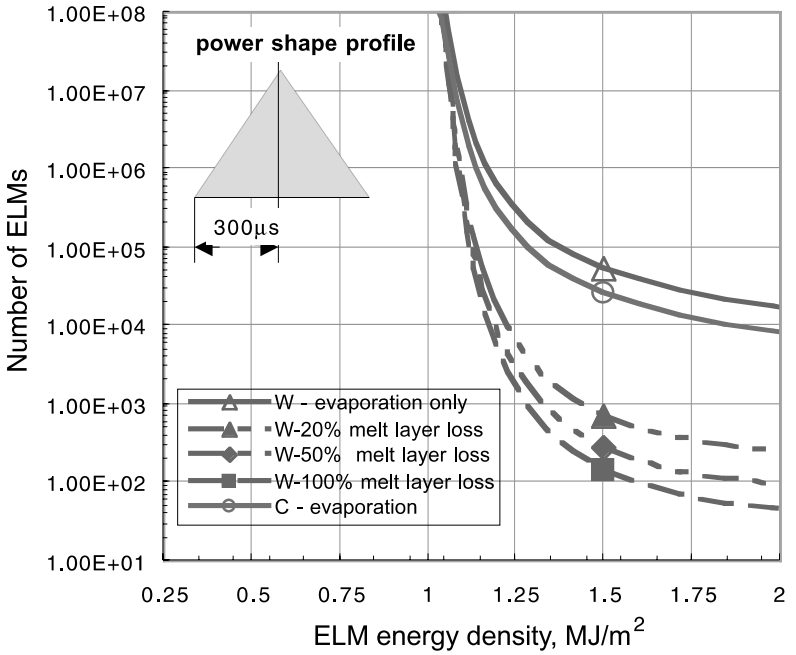

Fig. 1. Number of ELMs to erode 2 cm of C or 1 cm of W vs. ELM energy per unit area, for ELM thermal loads with a triangular power shape profile and with a rise and fall time of 0.3 ms and a peak heat flux in between ELMs of 5 MW m^{-2}. For C, brittle destruction effects are not included. For W, results are shown assuming 0%, 20%, 50% and 100% loss of melt layer.

Erosion calculations done with the model described in Refs. [24,25] show that the acceptable energy density is of the order of 1 MJ m^{-2} [23] (see also Fig. 1) assuming for ELM thermal loads a triangular power shape profile with a rise and fall time of 0.3 ms each. A large number of ELMs with energy densities >1 MJ m^{-2} would lead to an intolerably short erosion lifetime. More pessimistic conditions are found assuming shorter ELM duration and a square power load profile [26].

In ITER $W_{\rm ped} = 105$ MJ, $W_{\rm dia} = 350$ MJ, $T_{\rm ped} = 3.3$ keV and $\tau_{\|} = 240$ μs. By assuming consistently with ITER design calculations, a conservative value of 5 mm for the SOL power width at the plasma equator for steady heat flux in-between ELMs [27], the corresponding wetted area during ELMs (for a modest broadening of $\sim$1.5) is $\sim$4.6 m^2 for the reference design and $\sim$7.6 m^2 for a more inclined target. Assuming a broader SOL power width at the mid-plane, e.g., 10 mm, would lead to a larger wetted area: $\sim$9.3 m^2 with broadening for the reference target design and $\sim$15 m^2 for a more inclined target. According to experimental observations [29] discussed above we also assume a broadening during ELMs of $\lambda_{\rm ELM}/\lambda_{\rm ELM}^{\rm betw} \approx 1.5$, $\tau_{\rm IR}/\tau_{\|} \approx 1.6$, $\Delta W_{\rm ELM}^{\rm div}/\Delta W_{\rm ELM} \approx 0.65$. For tungsten, it is also assumed that, once the melt layer is formed, the fraction of melt loss is about 50%. Finally, in these calculations, we neglect any vapour shielding effect, which would reduce the incoming pulsed heat flux, and to first-order is expected only for ELM energies >1.5 MJ m^{-2}. The results of ELM erosion lifetime analysis carried out using these assumptions are shown in Fig. 2(a) for a 20 mm CFC target and (b) for a 10 mm thick tungsten target. As a part of a parametric analysis three cases were analysed: $\Delta W_{\rm ELM}/W_{\rm ped}$: 0.05, 0.1, 0.15. The results show that a sufficiently high number of Type I ELMs to give a tolerable erosion lifetime for the ITER divertor target (i.e., $>10^6$ ELMs), can only be achieved for both carbon and tungsten for up to $\Delta W_{\rm ELM}/W_{\rm ped} = 0.15$ (i.e., $\Delta W_{\rm ELM} = 15$ MJ), which is within the range of experimental observations in current machines, using an inclined target (see cases * in Fig. 2).

It must be noted that these analyses are more reliable for indicating trends, rather than providing firm quantitative predictions. Generally, carbon performs better than tungsten, although ELM erosion results for CFC are subject to uncertainties of the thermal properties (e.g., thermal conductivity) at very high temperatures where data are still meagre. Discrepancies with more pessimistic results of analysis presented in Ref. [28] are due to higher values for the thermal conductivity of CFC assumed here at high temperatures. It is also worth mentioning that particularly at high ELM energy densities (e.g., resulting from ELM energy losses >15 MJ) onset of vapour shielding effects, not included here, could, to some extent, mitigate erosion.

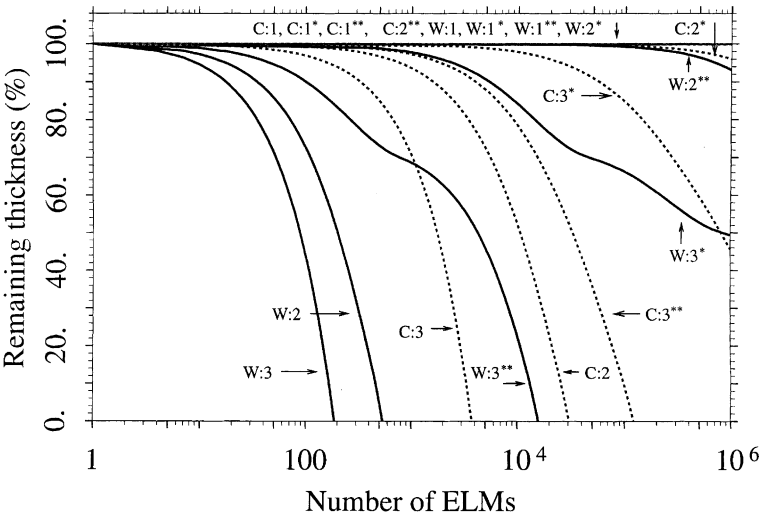

Fig. 2. Remaining thickness vs. number of ELMs for a CFC target (dotted lines) and W target (continuous line). The different curves refer to different assumed fraction of the pedestal energy loss during Type I ELMs (1) 5%, (2) 10% and (3) 15%. Cases without asterisk refer to a reference divertor geometry case with $\lambda = 5$ mm at the plasma equator, for a steady heat flux in-between ELMs of 5 MW m^{-2}. Cases * refer to 'steep' design target with $\lambda = 5$ mm. Cases ** refer to assumed a $\lambda = 10$ mm and a reference target design. Assumed $\tau_{IR} = \sim 400$ μs. Other assumptions are discussed in the text.

In addition, the statistical nature of the ELMs, whose characteristic parameters vary within a certain range from ELM to ELM, suggests that an analysis of the type discussed above, carried out by assuming a fixed set of average ELM parameters over a large number of events might not be sufficiently accurate. A statistic analysis would allow to account for erosion effects arising from ELMs, whose energy density and/or duration vary from the assumed average parameters. To this aim, a statistical erosion analysis, is underway based on using distributions of the variable of interest (i.e., ΔW_{ELM}, λ_{ELM}, τ_{IR}) in given experimental ranges derived from present machines [29]. The values of the energy loss to the divertor target per ELM, the wetted area, and the duration are in this case randomly determined for each ELM (within the ranges mentioned above) by a Monte Carlo technique. Once the energy density of the ELM and its duration are determined, ensuing erosion is calculated using the model mentioned above for an assumed power shape profile. As the target is eroded, the surface temperature, prior to the ELMs, is recalculated for the new thickness and then the procedure advances step-wise in time. Detailed descriptions of the computational methodology and of the analysis results are presented elsewhere [30].

More rigorous analysis of the ablation and melting processes during ELMs and their interplay with plasma shielding, and of the coupling between the plasma edge and the re-radiation from the impurity plasma, are also in progress using more sophisticated computational tools [31]. Preliminary results of these analyses are discussed elsewhere [32,33].

Alternative regimes to Type I ELMs are also being vigorously investigated in today's machines. The most promising regime is that with Type II ELMs, whose associated heat transient loads are much smaller than those of Type I ELMs, for similar pedestal and core plasma parameters (by at least a factor of 3–5) but a rigorous inter-machine comparison and extrapolation to ITER remains to be done [34–36].

3.2. Disruptions in ITER: effects and prospects for mitigation

Thermal quench of a full performance ITER plasma, with ~350 MJ of thermal energy and ~310 MJ magnetic energy, will result in significant transient heat loads, if localised at a narrow area of the divertor near the strike points, which must be accommodated by vaporisation and melting of sacrificial material. It will also cause electro-dynamic stresses on the first wall and surrounding structures.

Presently, we assume that for a worst-case ITER disruption thermal quench, the energy loss is 80–100% of the initial plasma thermal energy, the SOL width expands only modestly (e.g., three times), the inboard/outboard divertor energy ratio may vary between 2:1 and 1:2 and there is a toroidal energy peaking factor (peak/average ratio) up to 1.5 [37,38]. This would lead to >10 MJ m^{-2} at the target. For these conditions, a vaporisation layer of the order of few microns is expected

for both CFC and W [39–42]. In the case of tungsten a melt layer of few hundred microns could develop, part of which, if not all, could be lost.

However, the analysis of disruptions in present experiments, such as JET and ASDEX-Upgrade, shows that, typically, much less severe power loads are observed [43]. While the time evolution of the heat load is as expected, only a small fraction, typically $\leqslant 20\%$ of the stored energy, arrives in the divertor. Furthermore, the spatial distribution of the disruption heat load is >10-times broader than the original strike zones. If this is confirmed, energy densities resulting from disruptions in ITER would be much lower (typically 1–3 MJ m^2) than presently assumed and resulting erosion effects would be less severe. Further work in this area is needed (see Section 4).

While the first-wall and the divertor structures are being designed to withstand a limited number of worst-case disruptions, there is a strong incentive to reduce the disruption frequency and minimise the corresponding effects. Clearly, this must be also done for successful post-ITER commercial fusion reactors. The frequency of disruptions in ITER for full performance operation is assumed $\sim$10%. While these frequencies are consistent with present experiments, a justification for them in ITER requires continuing studies of the sensitivity of inherent disruptivity to the proximity of operational limits and careful analysis of data to separate the effects of administrative limits on disruptions and plasma operational objectives, procedures and operator experience from the underlying physics. The development and availability of sophisticated plasma and machine status diagnostics to provide a basis for disruption avoidance and onset warning in modes of operation near the limits, and of techniques to mitigate the severity of disruptions (e.g., see for example [44–46]), could relax some of design requirements for PFCs. This would have a very favourable implication on the use of a full W clad divertor in ITER.

3.3. Tritium co-deposition effects and control of the tritium inventory

Tritium issues will play a central role in the operation of ITER and the safety aspects associated with tritium will attract intense scrutiny. Although operation of existing C-lined tokamaks, together with focussed laboratory studies have illuminated the challenges, the quantification of tritium co-deposition with eroded carbon in ITER is still subject to large uncertainties. Sparse diagnostic coverage and low-dedicated experimental run time have hampered the validation and improvement of predictive models [47,48].

3.3.1. Divertor tritium co-deposition inventory analysis

The REDEP/WBC code package is being used to compute carbon chemical erosion and tritium co-deposition for the ITER carbon divertor target. Refs. [6,49] discuss erosion/redeposition code validation. A case from B2-EIRENE with plasma fuelled mostly by gas puffing from the top of the plasma at a rate of 110 Pa m^{-3} s^{-1} was selected for this analysis (see Fig. 3(c)). It represents the reference ITER option of a carbon-clad target with 100 MW entering the scrape-off-layer (SOL). Since the available models of ELMs do not yet allow predictive modelling, results of steady-state modelling representing values time-averaged over many ELM periods have been used [5,50].

Analysis was made assuming surface temperature profiles along the target calculated from the background plasma power fluxes. The model [51] for a DT chemical sputtering yield as a function of particle energy and surface temperature was used for the carbon erosion calculations.

Chemically eroded carbon erosion/redeposition models in REDEP/WBC have recently been upgraded [52]. These upgrades include MOLDYN molecular dynamics code calculations of carbon/hydrocarbon reflection on a hydrogen-saturated carbon surface [52,53]. These calculations show lower sticking of redeposited carbon than previously assumed, at detached-plasma-relevant low-incident energies ($\sim$1–20 eV).

A number of simplifications were used in the present analysis. These include area scaling of outer divertor plate results for the full (inner and outer) divertor system, simplified treatment of MOLDYN code reflection output (e.g., reflected species = incident species only), simplified treatment of carbon material lost from the divertor (no detailed treatment of where some of this material ends up), and certain plasma approximations, e.g., regarding neutral fluxes. Also, since the chemical yield model was developed for 800 °C maximum surface temperature, divertor temperatures higher than this used the 800 °C yield value.

For the WBC analysis, 100 000 chemically eroded hydrocarbon molecules were launched, along the detached-plasma portion of the outer divertor target. The molecules launched range from methane to propylene [54] in accordance with UTIAS data [55]. The calculation is fully kinetic, 3-D, with sub-gyro orbit motion. Particles are launched corresponding to a thermal distribution at the local surface temperature. A particle then undergoes charge-changing and velocity-changing collisions with the plasma, including proton and electron ionisation, dissociation, recombination, charge exchange, elastic collisions with the incoming plasma, and (charged particle) sheath electric field acceleration. Particles redepositing on the divertor surface stick or reflect per the molecular dynamic code results. All carbon-containing particles are followed, i.e. hydrocarbon molecules and molecular ions, radicals, and carbon atoms and ions. A particle history terminates upon sticking to the divertor surface or being lost from the

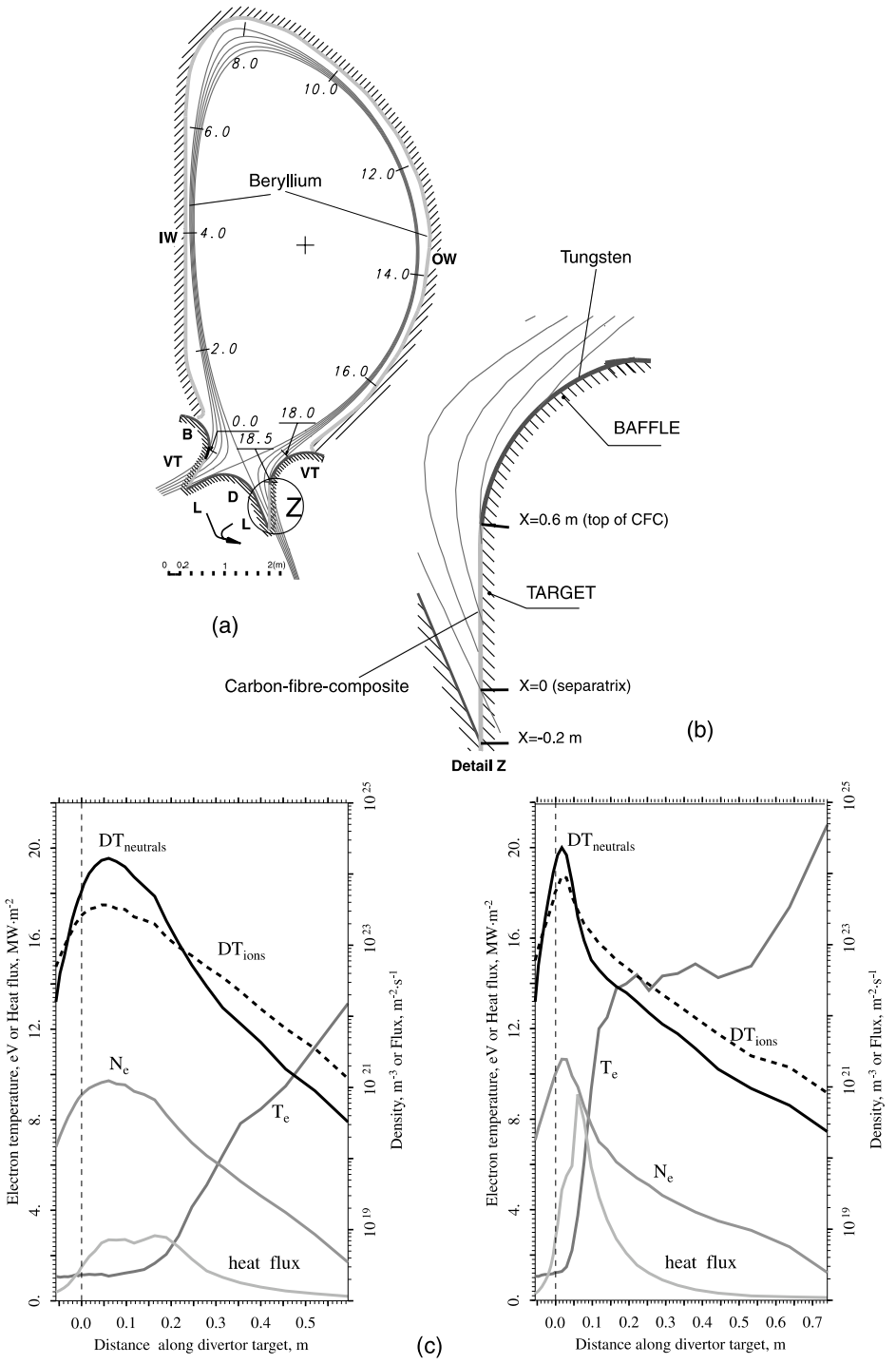

Fig. 3. (a) ITER poloidal cross-section showing inner (IW) and outer (OW) first-wall, divertor vertical target (VT), divertor baffle (B), and divertor private region consisting of dome (D), and liner (L). Start-up limiters (two modules) are located at the equatorial level. SOL magnetic surfaces including separatrix are shown (the outermost surface delimits the EIRENE calculation grid, numbers are distance in metres along this line). (b) Detail of the divertor target. (c) Plasma temperature, density, particle and heat fluxes along the ITER outer divertor target for a reference semi-detached edge plasma. Left: inner divertor target: right: outer divertor target.

near-surface calculational volume. Tritium co-deposition is computed based on regions of net carbon growth.

The peak net erosion rate is $\sim$20 nm s^{-1} (gross erosion rate 105 nm s^{-1}), occurring in a small region near the strike points. The computed tritium co-deposition rate is <10 gT/1000 s (i.e., <4 gT/pulse). This is about a factor of three higher than for a unity-sticking assumption. If confirmed by further dedicated experimental and modelling work and direct operation experience with D in ITER (see Section 4), this rate of co-deposition, albeit smaller than observed in machines like JET, will require use of efficient in situ tritium removal techniques, to meet the safety imposed in-vessel tritium co-deposition limits and/or for fuel supply economy reasons.

3.3.2. Estimates of charge exchange neutrals and ion erosion of the ITER first wall during full DT burn operation

Erosion of the beryllium first-wall due to physical sputtering by charge exchange DT neutrals from plasma recycling and gas puffing, and by DT and impurity ions (e.g., He, C) or externally seeded impurities (e.g., Ar), was calculated using the methodology described elsewhere [28]. Two different background plasma solutions from B2-EIRENE were considered: (i) with a carbon divertor (see above); (ii) with a tungsten divertor and Ar seeding. In order to evaluate the neutral fluxes, the EIRENE code was run stand-alone with modifications ensuring accurate computation of the energy spectra of the neutrals impinging upon the surface.

The results of these analyses and the subsequent transport of eroded material onto the divertor surfaces, are summarised in Table 1. Additional information on this subject can be found elsewhere [56].

The beryllium peak erosion rate for both cases analysed is $\sim$0.1 nm s^{-1} is acceptable for the low-duty-factor operation of ITER. Tungsten erosion would be two orders of magnitude lower. The total eroded Be flux integrated over the entire ITER first-wall is estimated to be $\sim 2.8 \times 10^{21}$ s^{-1} (about 1/3 of that for an oxidised Be wall). A carbon wall would yield a net erosion flux similar to Be (see Table 1).

The Be eroded from the first wall will migrate to the divertor surfaces exposed to the plasma. As a matter of fact, beryllium is not eroded chemically and, once deposited, has a high-sticking probability. Thus, the migration path of beryllium is restricted to much smaller distances and cannot reach the remote areas. This in ITER will certainly lead to the formation of beryllium-rich films that could substantially reduce carbon chemical erosion and the consequent tritium co-deposition. Further experiments to elucidate these effects are being planned in the linear plasma simulator PISCES-B [57]. However, the beryllium-rich surface layer, if any, would tend to be removed periodically by ELMs and disruptions. On the other hand, Be arriving at the divertor may contribute, in the presence of oxygen, to some co-deposition in the divertor. The resulting worst-case co-deposition rates, resulting from material eroded from the wall, assuming that the material builds up in lower temperature areas of the divertor (see operation experience at JET [58]), are also shown in Table 1.

3.4. Efficiency of edge and core fuelling for expected n_{ped} in ITER

The pedestal density is essentially determined by the ionisation of thermal neutrals from the edge in combination with the reduction of transport in the pedestal. The required source rate from edge fuelling in machines like ASDEX-Upgrade and JET agrees with B2-EIRENE modelling. However, modelling with the ASTRA Code [59] shows that the fuelling rate required for high-fusion power operation of ITER, if provided by edge fuelling alone, is almost an order of magnitude larger than that from edge fuelling which can be supplied through the

Table 1
First-wall erosion and resulting tritium co-deposition rates in the divertor[a]

	(i) With carbon			(ii) With externally seeded impurities		
	Peak (average) erosion rate δ_M (μm/400 s)	Mass eroded δ_M (g/400 s)	T-codep. rate δ_T (g/400 s)	Peak (average) erosion rate δ_M (μm/400 s)	Mass eroded δ_M (g/400 s)	T-codep. rate δ_T (g/400 s)
Be	0.027 (1.3×10^{-2})	17	0.1 (T/Be $\sim$ 0.05)	0.03 (1.3×10^{-2})	16	0.1 (T/Be $\sim$ 0.05)
BeO[b]	0.016 (4.1×10^{-3})	5.3	0.1 (T/BeO $\sim$ 0.1)		Not calculated	
W[b]	2×10^{-3} (1.2×10^{-3})	16	0	2×10^{-3} (1.7×10^{-3})	22	0
C[b]	0.016 (1.7×10^{-2})	24	>1	0.017 (1.6×10^{-2})	23	>1

[a] It is assumed that this material will be transported to the divertor.
[b] Shown only for comparison.

scrape-off layer according to B2-Eirene simulations [50]. With gas-puffing only, a high-pedestal density ($n_{ped} \approx (7–9) \times 10^{19}$ m^{-3}) cannot be achieved even assuming a particle diffusion coefficient as low as the neo-classical level (≈ 0.06 m^2 s^{-1}), since only a small fraction of gas-puffed neutrals can penetrate across the separatrix due to a thicker SOL in ITER than in present machines. Therefore, core fuelling is mandatory in ITER. Fig. 3 in Ref. [60] shows the achievable pedestal density for a case with rather a high-diffusion coefficient (≈ 0.3 m^2 s^{-1}) and a reduced diffusion coefficient (≈ 0.06 m^2 s^{-1}) with an assumed core fuelling rate of 14 Pa m^3 s^{-1} and 28 Pa m^3 s^{-1}, respectively. In this calculation, the width of the pedestal is assumed to be $\sim$10 cm. Injection of particles within the pedestal region (pedestal fuelling) can also provide the necessary pedestal density for ITER, albeit, in this case, the efficiency of density increase is lower compared with core fuelling.

High-field side pellet injection (50–100 Pa m^3 s^{-1} and deposition depth = 0.15 a with 500 m s^{-1}) is used in ITER to meet these core fuelling requirements. Recent calculations [61] using the ASTRA transport code with a cloud-charging model [62] for the pellet ablation and a simplified expression for the ablated mass relocation based on reduced MHD [63], showed that high-field side injection with rather small velocities ($\approx$100–300 m s^{-1}) could provide deep fuelling beyond the pedestal region.

3.5. Preliminary estimates of W erosion and transport in ITER during normal operation

In anticipation of positive developments in disruption and ELM mitigation, a high-heat-flux tungsten vertical target is being considered as a possible alternative in ITER.

The erosion of W in the divertor due to physical sputtering during normal operation and its transport in the SOL are recognised to be important problems. Results from the ASDEX-Upgrade W-divertor experiment showed that the erosion of tungsten was dominated by impurities and that the erosion yield as well as the transport in the main chamber critically depended on the actual divertor plasma parameters [64]. Preliminary modelling results are discussed in this paper using DIVIMP [65] with a background plasma solution from B2/EIRENE for a case with a partially detached divertor plasma seeded by argon, for radiation cooling, which is introduced via gas puff in the private-flux region. In this case the input power is 130 MW, $n_s = 3.2 \times 10^{19}$ m^{-3} and $q_{pk} = 8$ MW m^{-2}. We also assume only physical sputtering produced by Ar ions at normal incidence. The resulting sputtered W flux was calculated taking into account the fluxes of all ionization stages of argon. The sputtering data was taken from [66], the ionization and recombination cross sections for W in DIVIMP are taken from a modified ADPAK data base [67]. The W transport in the SOL was computed using the same parameters as in the B2/EIRENE background plasma, i.e. $D_\perp = 0.3$ m^2 s^{-1} and no drifts. Poloidal flows were not included.

The resulting W concentrations are shown in Fig. 4 for the divertor region and for the whole SOL plasma. The concentration of tungsten is especially high in some parts of the divertor, in the inner divertor even relatively far away from the divertor plates. However, in the confined plasma inside the separatrix it is below 5×10^{-6}, which would be tolerable for ITER (maximum allowable core concentration $\sim 2 \times 10^{-5}$). In all, the present analysis must be regarded as highly uncertain and further work is required to improve predictions (see Section 4).

4. Main uncertainties and future R&D priorities

The issues that require further urgent work were discussed in detail elsewhere [6] and here we highlight only the topics with highest priority.

Divertor thermal loads during ELMs: Further experiments in tokamaks and modelling are urgently needed to better understand how the plasma energy is distributed during Type I ELMs (e.g., SOL broadening effects, movements of the separatrix, heat and particle transport, duration and shape of the power load profiles). If a significant part of the ELM energy flows to the main chamber walls, this would ease the divertor ELM erosion problem, but may exacerbate the erosion of the main chamber walls and plasma contamination by main-chamber produced impurities. While further work certainly needs to study Type I ELMs, other options should also be explored. In particular, it is important to expand studies of regimes free of Type I ELMs (e.g., with Type II ELMs), which are compatible with required confinement, to determine if their operational space can be exploited in ITER.

Disruptions: Dedicated work is required in tokamaks to improve understanding of disruption parameters: fraction of energy lost to the (inner/outer) divertor and to the wall; location and duration of impact, wetted area including SOL broadening effects, time evolution of the power load, etc. Efforts to reduce transients and to mitigate disruptions must continue at the highest priority. Behaviour of melt layer formed during ELMs and disruptions remains a topic of ongoing research.

Predictions of tritium co-deposition and control of the in-vessel inventory: Unlike for physical sputtering and/or higher edge plasma temperature regimes, where good code/data validation exists, the erosion/redeposition codes are not well validated for detached conditions. In fact, there is a large discrepancy between code/data results for JET, with the codes under-predicting co-deposition by factors of roughly 10–40, possibly due to much

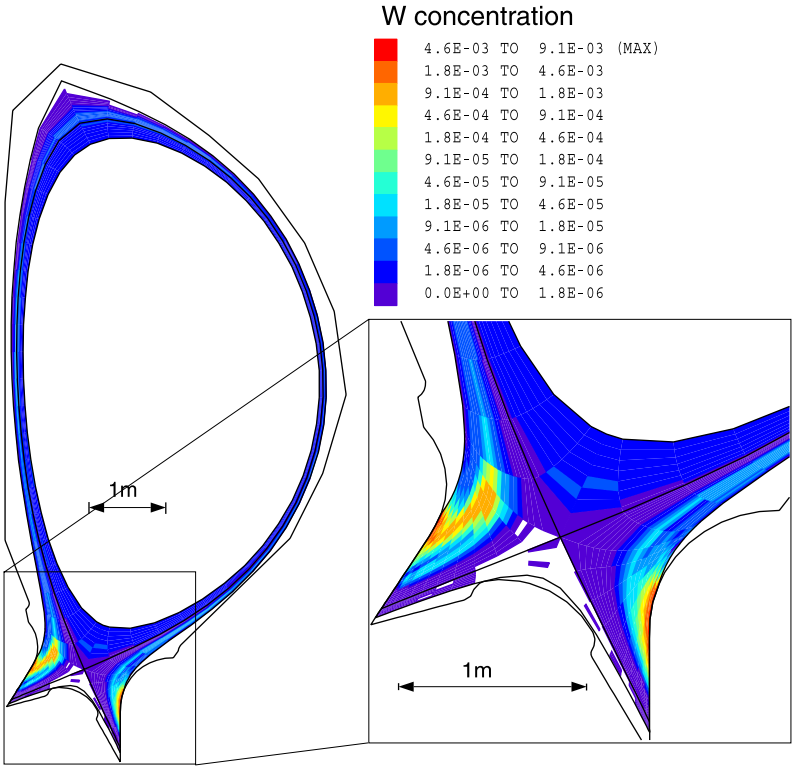

Fig. 4. DIVIMP modelling of the poloidal distribution of the W concentration in the divertor of ITER.

larger chemical erosion yields from soft, D-containing redeposited carbon films [52,68,69]. On the other hand, such higher yields are not apparent in PISCES-B or DIII-D data. Also, unlike JET, ITER has a beryllium wall and not a carbon wall.

Fuelling: Further work needed in this area includes improved understanding of the particle transport processes within the pedestal region, identification of the relation between the density limit due to complete divertor detachment and achievable pedestal density, quantification of the pellet effect on the ELM triggering and its size.

Issues with erosion and transport of W: Clearly, the reliability of the results presented here cannot be better than the simplified plasma solution used (e.g., no drifts, no ELMs, etc.). Another effect which is not included here, and might be important, is the friction between Ar and W. Overall, code/data validation is still very scarce and additional modelling efforts in this direction are needed using data available from ASDEX-Upgrade [64,70,71].

5. Conclusions

This paper has discussed some of the remaining crucial plasma edge physics and PMI issues of the ITER tokamak and progress with their resolution, using either modelling or projections of experimental results from existing tokamak operation or relevant laboratory simulations. A sufficiently clear understanding of these issues is challenging and requires a co-ordinated R&D effort, involving extensive participation by all parts of the fusion community.

The projection of heat loads due to Type-I ELMs in ITER, and the ensuing erosion as well as the control of tritium co-deposition with eroded carbon are still uncertain. Calculations discussed in this paper show that by further inclining the divertor target and increasing the wetted area (e.g., using a factor of two smaller poloidal angle of magnetic field lines at the target surfaces), ~10–15 MJ per ELM pulse could be tolerated, particularly with a C target, which are within the range of experimental observations in current machines. But, this improvement comes at the expenses of a reduced plasma shape flexibility. More rigourous analysis based on a statistical approach are in progress and may lead to more unfavourable erosion lifetime results. Furthermore, extension of the lifetime of the target plates is possible e.g. by operation with more benign Type II ELMs with a small decrease of plasma current.

The use of carbon in ITER will lead to tritium co-deposition and operational availability of the machine will depend on the availability of reliable tritium co-deposition mitigation and/or removal techniques, which

still need to be developed. An important uncertainty, which is being addressed by R&D, is whether the deposition of eroded Be from the wall at the target plate could reduce substantially carbon erosion and, thus, co-deposition.

Based on the recent advances in areas such as mitigation of disruption effects and regimes with smaller ELMs, a promising path is opening up for using a full W plate in ITER.

There have been remarkable advances in experiments and theory, but the uncertainties are likely to remain – such that ITER needs to be operated to quantify the effects and the resulting implications on plasma performance and operation with sufficient precision. The ITER design has enough built-in flexibility and the anticipated staged operation strategy will allow for further optimisation/modification of the design and operation. In particular, the initial phase of operation with H- and D-plasmas will permit to explore these problem areas, and better quantify the resulting effects and the attendant uncertainties. If necessary, some remedial actions or mitigation techniques can be implemented to off-set possibly underestimated or unforeseen phenomena (e.g., an operational regime with smaller than Type I ELMs and good confinement, techniques to mitigate disruption effects, design optimizations to mitigate occurrence of co-deposition in areas remote from the plasma, or elimination of carbon). Plasma edge and wall diagnostics in ITER, and adequate models sufficiently benchmarked against experiments, will be an essential element to implement this strategy.

Acknowledgements

The authors would like to acknowledge many fruitful discussions with several scientists in the fusion community including work by US co-authors supported by the US Department of Energy, Office of Fusion Energy.

This report was prepared as an account of work undertaken within the framework of ITER Co-ordinated Technical Activities (CTA). These are conducted by the Participants: Canada, the European Atomic Energy Community, Japan, and the Russian Federation, under the auspices of the International Atomic Energy Agency. The views and opinions expressed herein do not necessarily reflect those of the Participants to the CTA, the IAEA or any agency thereof. Dissemination of the information in this paper is governed by the applicable terms of the former ITER-EDA Agreement.

References

[1] ITER EDA Agreement and Protocol 2, ITER EDA Documentation Series No. 5, IAEA, Vienna, 1994.
[2] ITER Technical Basis, ITER EDA Documentation Series No. 24, IAEA, Vienna, 2002.
[3] V. Mukhovatov et al., Comparison of ITER performance predicted by empirical, semi-empirical and theory-based transport models, 19th IAEA Fusion Energy Conference, Lyon, France, 14–19 October 2002.
[4] A. Kukushkin, 28th EPS Conf. on Contr. Fusion and Plasma Phys., Funchal, 18–22 June 2001, P5105, ECA, vol. 25A (2001) 2113.
[5] H.D. Pacher et al., these Proceedings. PII: S0022-3115(02)01374-0.
[6] G. Federici, C.H. Skinner, et al., Nucl. Fusion 41 (2001) 1967.
[7] R. Parker et al., J. Nucl. Mater. 241–243 (1997) 1.
[8] G. Janeschitz et al., Nucl. Fusion 40 (2000) 1197.
[9] I. Arkhipov et al., J. Nucl. Mater. 290–293 (2001) 394.
[10] A. von Keudell, T. Schwarz-Selinger, W. Jacob, A. Stevens, J. Nucl. Mater. 290–293 (2001) 231.
[11] A. Makhankov et al., Fusion Eng. Des. 49–50 (2000) 275.
[12] C. Ibbott et al., Fusion Eng. Des. 56–57 (2001) 243.
[13] A.W. Leonard, J. Nucl. Mater. 266–269 (1999) 109.
[14] A. Loarte et al., Proc. 18th Int. Conf. Sorrento, 2000, IAEA, Vienna, 2001, IAEA-CN-77. CD-ROM file ITERP/11(R), and http://www.iaea.org/programmes/ripc/physics/fec2000/html/node245.htm#55022.
[15] A. Loarte et al., these Proceedings. PII: S0022-3115(02)01398-3.
[16] G. Janeschitz, J. Nucl. Mater. 290–293 (2001) 1.
[17] A. Leonard, J. Nucl. Mater. 241–243 (1997) 628.
[18] A. Herrmann, Plasma Phys. Contr. Fusion 37 (1995) 17.
[19] A. Herrmann, these Proceedings. PII: S0022-3115(02)01422-8.
[20] T. Eich, these Proceedings. PII: S0022-3115(02)01477-0.
[21] G. Counsell, IAEA TCM Workshop on Divertor Concepts, Plasma Phys. Contr. Fusion 44 (2002) 827.
[22] G.Y. Antar, S.I. Krasheninnikov, P. Devynck, et al., Phys. Rev. Lett. 87 (2001) 065001.
[23] G. Federici, H. Wuerz, G. Janeschitz, R. Tivey, Erosion of plasma facing components in ITER, Fusion Eng. Des., in press.
[24] A.R. Raffray, G. Federici, J. Nucl. Mater. 244 (1997) 85.
[25] G. Federici, A.R. Raffray, J. Nucl. Mater. 244 (1997) 101.
[26] G. Federici et al., Selection of Plasma-Facing Materials in Next-Step Fusion Devices, 19th Symposium on Fusion Engineering, SOFE, January 22–25, 2002, Atlantic City, NJ, IEEE02CH37231 (2002) 311.
[27] A.S. Kukushkin et al., J. Nucl. Mater. 290–293 (2001) 887.
[28] G. Federici et al., J. Nucl. Mater. 290–293 (2001) 260.
[29] A. Loarte, these Proceedings. PII: S0022-3115(02)01398-3.
[30] G. Federici, A. Loarte, G. Saibene, P. Barabaschi, Estimates of ELM erosion in ITER using a statistical approach, Fusion Sci. Technol., to be submitted.
[31] H. Wuerz et al., Fusion Sci. Technol. 40 (2001) 191.
[32] H. Wuerz et al., J. Nucl. Mater. 290–293 (2001) 1138.
[33] S. Pestchanyi, H. Wuerz, I. Landman, IAEA-TCM on Divertor Concepts Cadarache Sept 2001, Plasma Phys. Contr. Fusion 44 (2002) 845.
[34] Y. Kamada, Plasma Phys. Contr. Fusion 42 (2000) A247.
[35] J. Stober et al., Nucl. Fusion 41 (2001) 1123.
[36] G. Saibene, Plasma Phys. Contr. Fusion 44 (2002) 1769.

[37] J. Wesley, N. Fujisawa, S. Putvinski, M.N. Rosenbluth, Assessment of disruption and disruption-related physics basis for ITER, in Fusion Engineering 1997 Proc. 17th Symp. San Diego, 1997, Vol. 1, IEEE, Piscataway, NJ, 1998, p. 483.
[38] ITER Physics Basis, Nucl. Fusion 39 (1999) 2137.
[39] H. Wuerz, S. Pestchanyi, B. Bazylev, F. Kappler, A consistent 2D analysis of the ITER 2D divertor, in: Proc. 20th Symp. Fus. Technol., Marseille, France, Vol. 1, 1998, p. 271.
[40] H. Wuerz et al., Fusion Eng. Des. 56–57 (2001) 349.
[41] H. Wuerz et al., Report Forschungszentrum Karlsruhe, FZKA 6582, 2001.
[42] A. Hassanein, I. Konkashbaev, J. Nucl. Mater. 273 (1999) 326.
[43] P. Andrew et al., these Proceedings. PII: S0022-3115(02)01586-6.
[44] P.L. Taylor et al., Phys. Plasmas 6 (1999) 1872.
[45] G. Pautasso et al., J. Nucl. Mater. 290–293 (2001) 1185.
[46] D. Whyte et al., these Proceedings. PII: S0022-3115(02)01525-8.
[47] G.F. Counsell et al., J. Nucl. Mater. 290–293 (2001) 255.
[48] V. Rohde et al., these Proceedings. PII: S0022-3115(02)01335-1.
[49] J.N. Brooks, Fusion Eng. Des. 60 (2002) 515.
[50] A.S. Kukushkin, H.D. Pacher, Plasma Phys. Contr. Fusion 44 (2002) 931.
[51] G. Federici et al., J. Nucl. Mater. 266–269 (1999) 14.
[52] J.N. Brooks et al., these Proceedings. PII: S0022-3115(02)01405-8.
[53] D.A. Alman et al., these Proceedings. PII: S0022-3115(02)01428-9.
[54] J.N. Brooks, D.A. Alman, G. Federici, D.N. Ruzic, D.G. Whyte, J. Nucl. Mater. 266–269 (1999) 58.
[55] B.V. Mech, A.A. Haasz, J.W. Davis, J. Nucl. Mater. 255 (1998) 153.
[56] R. Behrisch et al., these Proceedings. PII: S0022-3115(02)01580-5.
[57] R. Doerner, private communication.
[58] F. Scaffidi-Argentina et al., J. Nucl. Mater. 307–311 (2002) 1411.
[59] G. Pacher et al., Proceeding of the EPS Conf. 2001, Madeira Portugal, P2.037.
[60] M. Sugihara, J. Plasma Fusion Res., in press.
[61] A.R. Polevoi, M. Shimada, Plasma Phys. Contr. Fusion 43 (2001) 1525.
[62] B. Kuteev, Nucl. Fusion 35 (1995) 431.
[63] H.R. Strauss, W. Park, Phys. Plasmas 5 (1998) 2676.
[64] K. Krieger et al., J. Nucl. Mater. 266–269 (1999) 207.
[65] P.C. Stangeby, J.D. Elder, J. Nucl. Mater. 196–198 (1992) 258.
[66] W. Eckstein et al., Sputtering Data IPP 9/82, 1993.
[67] K. Asmussen et al., Nucl. Fusion 38 (1998) 7.
[68] V. Philipps et al., these Proceedings. PII: S0022-3115(02)01344-2.
[69] A. Kirschner et al, Hydrocarbon transport in the MkIIa divertor of JET, Plasma Phys. Contr. Fusion, in press.
[70] R. Neu, these Proceedings. PII: S0022-3115(02)01386-7.
[71] A. Geier et al., these Proceedings. PII: S0022-3115(02)01519-2.